

AIST: An Interpretable Attention-based Deep learning Model for Crime Prediction

YEASIR RAYHAN, Bangladesh University of Engineering and Technology, Bangladesh

TANZIMA HASHEM, Bangladesh University of Engineering and Technology, Bangladesh

Accuracy and interpretability are two essential properties for a crime prediction model. Because of the adverse effects that the crimes can have on human life, economy and safety, we need a model that can predict future occurrence of crime as accurately as possible so that early steps can be taken to avoid the crime. On the other hand, an interpretable model reveals the reason behind a model's prediction, ensures its transparency and allows us to plan the crime prevention steps accordingly. The key challenge in developing the model is to capture the non-linear spatial dependency and temporal patterns of a specific crime category while keeping the underlying structure of the model interpretable. In this paper, we develop AIST, an Attention-based Interpretable Spatio Temporal Network for crime prediction. AIST models the dynamic spatio-temporal correlations for a crime category based on past crime occurrences, external features (e.g., traffic flow and point of interest (POI) information) and recurring trends of crime. Extensive experiments show the superiority of our model in terms of both accuracy and interpretability using real datasets.

CCS Concepts: • **Information systems** → *Spatial-temporal systems*.

Additional Key Words and Phrases: Spatio-temporal prediction, crime prediction, interpretability, attention

1 INTRODUCTION

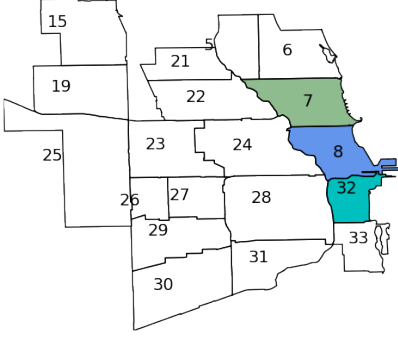
Criminal activities have become a major social problem due to their adverse effect on human life, economy and safety. The availability of crime data in recent years has enabled researchers to develop models for crime prediction. The government and responsible authorities can take preventive measures if they know about a crime event in advance. Knowing the insight behind the prediction of a crime occurrence would allow them to plan preventive measures appropriately and keep the society safe from the happening of the crime. Interpretable predictions ensure the transparency and accountability of the model. Thus, both accuracy and interpretability are two essential and desired properties for a crime prediction model. We propose an *Attention-based Interpretable Spatio Temporal Network (AIST)*, an interpretable deep learning model for crime prediction.

Crime events exhibit spatial and temporal correlations and external features (e.g., taxi flow) often have influence on the crime occurrence.

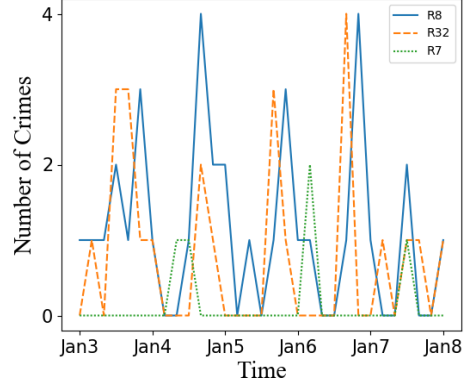
Spatial Correlation. Spatially nearby regions show a similar crime distribution and the extent of this similarity varies across regions and time. Figure 1b shows an example on January, 2019 Chicago crime data. Regions 8 and 32 show strong spatial correlation while Regions 8 and 7 do not, though both of them are spatially nearby. Also, the spatial correlation between Regions 8 and 32 changes with time.

Temporal Correlation. Crime occurrences of a region show both short and long term temporal correlation and these correlations vary with crime categories. Fig 2a shows an example for Region 8: deceptive practice (C1) and theft (C2) peak during late night and midnight, whereas robbery (C3) peak during early morning.

External Features. Functionalities and urban characteristics of a region like points of interests (POIs), traffic flow have direct influence on its crime occurrences. The influence of these external factors on crime tend to vary from time to time and region to region. Figure 2 shows an example, where the distribution of deceptive practice (C1) and theft (C2) (Figure 2a) is correlated to traffic outflow (Figure 2b) during evening but there is no correlation between robbery (C3) and traffic outflow or inflow.

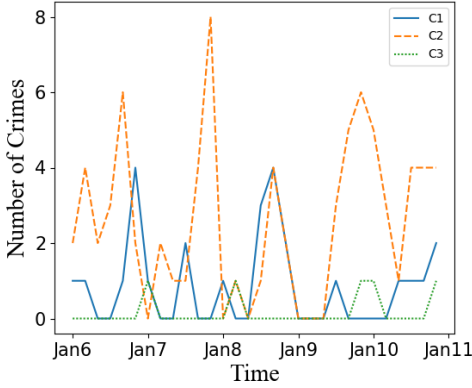


(a) Chicago Communities

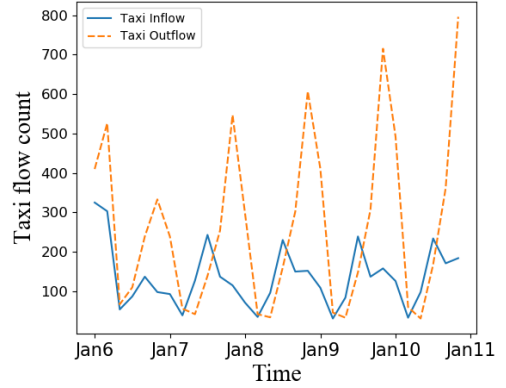


(b) Spatial correlation

Fig. 1. Spatial Dependencies of Chicago Communities



(a) Region 8 Crime Distribution



(b) Region 8 Taxi Flows

Fig. 2. Temporal and External Feature Correlation

Modeling these diverse spatio-temporal correlations and learning meaningful external features and their probable influence on crime are challenging tasks. For crime prediction, it is also necessary to keep the model’s architecture reasonably interpretable, which makes the tasks even harder than building a spatio-temporal model that does not consider interpretability [40].

Traditional interpretable machine learning and data mining methods [9, 50, 57] cannot model these non-linear spatio-temporal correlations and thus fail to predict the crime occurrences accurately. Recent deep learning models [22, 23] capture this non-linear spatial and temporal dependencies to some extent and improve the accuracy of traditional models. They still have major limitations:

- The models only learn static spatial correlations. However, the correlations for two regions may vary with time.
- The models do not address long term (e.g. daily, weekly) temporal correlations.

- The models do not consider the external features and hence the learned region embedding is incomplete.
- The models lack interpretability. Both these models use LSTM based attention weights which are difficult to interpret because of the recurrence on the hidden states generated by LSTMs [11]. They are also not sparse enough to be meaningful for long sequence.

To overcome the limitations, we develop AIST that captures dynamic spatio-temporal correlation for crime prediction and provides quantitative insights based on external features behind a prediction. We develop two novel variants of graph attention networks (GAT) [47], *hGAT* and *fGAT* to learn the crime and feature embedding of the nodes (regions), respectively at each time step. These embedding are then fed to three sparse attention based-LSTMs (SAB-LSTMs) [27] for modeling recent, daily and weekly crime trends. Finally, AIST applies a location-based attention mechanism to identify the significance of different trends to make a prediction.

GAT does not consider the hierarchical information of nodes. However, in real-world scenarios nodes tend to form clusters and belong to different hierarchies based on similar characteristics. In urban context, nodes (regions) that belong to a same hierarchy shares similar functionalities and crime distributions. We propose *hGAT* that incorporates this prior knowledge of hierarchical information into GAT’s architecture to produce a better crime embedding of nodes.

Concatenating the feature vectors with spatial [55, 56] or temporal view [30] either directly or after a linear transformation is a common practice for incorporating the external features into the model. However, it fails to fully utilize the features and generate insights for a model’s prediction. We propose *fGAT* that replaces the additive self-attention mechanism with a novel scaled dot product self-attention mechanism [46] to learn crime and region specific relevant feature embedding.

AIST is interpretable because it takes a transparent decision at each prediction step. To explain a prediction, we first find whether the prediction is based on recent occurrences or any recurring trend and then identify the previous time steps that are given the most importance. Our model knows why a time step is given importance as the input at each time step is an interpretable spatial embedding. Hence, if we backtrack we can find the most important regions and features for a specific time step.

Besides inherent interpretable architectures [7], recently post-hoc local explanation techniques [31] that provide approximate explanations to a model’s decision making have been explored to imitate the behavior of deep learning black box models. However, they are not well received considering the fact that if these explanations had been adequate enough, there would be no need for the original model [40]. Hence, we keep AIST architecture inherently interpretable while ensuring its accuracy.

In summary, the contributions of this paper are as follows:

- We propose a novel interpretable spatio-temporal deep learning model, AIST which is able to capture diverse spatio-temporal correlations based on past crime occurrences, external features and recurring trends.
- We propose *hGAT*, a novel GAT variant that allows AIST to learn more faithful node embedding.
- We propose *fGAT*, another novel GAT variant that provide insights behind the predictions of AIST.
- We conduct experiments on Chicago crime data. AIST achieves a higher accuracy than the state-of-the-art methods and provides useful insights for its predictions.

The remaining of the paper is organized as follows. We discuss the related work in Section 2 and formulate the crime prediction problem in Section 3. We present our model, *AIST* in Section 4.

Section 5 presents the experimental results and evaluates the accuracy and the interpretability of AIST. Section 6 concludes the paper.

2 RELATED WORK

Data-driven crime prediction problems have received wide attention from the researchers for decades. Existing studies on crime prediction can be divided into following categories: (i) *crime rate inference* that predicts the crime rate of a region, (ii) *crime hotspot detection* that finds the locations where crimes are clustered, and (iii) *crime occurrence prediction* that forecasts the occurrence of a crime category for a location at a future timestamp. Our work falls in the third category. In Sections 2.1 and 2.2, we elaborate existing crime prediction models and interpretable models, respectively. In Section 2.3, we discuss the deep learning methods used for spatial-temporal prediction.

2.1 Crime Prediction Models

Statistical and Classic Machine Learning Methods. Recent studies [41, 50, 51] used statistical and classic machine learning methods (e.g., linear regression, negative binomial regression, geographically weighted regression, random forest) for crime rate inference problem. In [50, 51], the authors studied the effect of point of interest (POI) (e.g., a restaurant or a shopping mall) and taxi flow information along with the traditional demographics features of a region while in [41], the authors utilized FourSquare check-in data for estimating the crime rate of a particular region. Researchers have also employed kernel density estimation (KDE) [5, 15, 16, 21] for predicting hot-spot maps. However, these works only take spatial features and dependencies into account ignoring the temporal dynamics of crime.

To address the temporal dynamics, time-series models such as autoregressive integrated moving average (ARIMA) [9] have been proposed for one-week ahead crime occurrence prediction. In [35], the authors implemented a self-exciting point process similar to one used by the seismologists in the context of urban crime to understand the temporal trends of burglary. Even though these models acknowledge the temporal dynamics, they do not incorporate the spatial context of crimes.

Both spatial and temporal information have been also explicitly modeled in the literature. In [57], the authors proposed an algorithm that constructs a global crime pattern from local crime cluster distributions, and employed it for predicting residential burglary. In [37], the authors employed STKDE, a variant of KDE for mapping transient and stable crime clusters. The work in [44] used analytic and statistical techniques to identify the spatio-temporal crime patterns. In [60], spatio-temporal correlations like intra-region temporal correlation and inter-region spatial correlation have been considered for crime occurrence prediction. However, all of these methods cannot fully model the complex non-linear relation of space and time and the dynamicity of spatial-temporal correlation.

Besides spatio-temporal features, incorporating additional data (e.g. Twitter, demographics data) improve the accuracy of existing crime prediction models. The authors in [19] added Twitter-based features extracted from topic based modeling for improving the prediction of models. In [4], the authors used fuzzy association rule mining to find consistent crime patterns using population demographics information of communities. Another line of work [49, 53] explores the heterogeneous and task-specific division of spatial regions over traditional grid and community based division which helps improve the accuracy of the crime prediction.

Deep Learning Methods. Deep learning models have recently been shown to be very effective in domains like computer vision, speech recognition and natural language processing. Recent deep learning models have also attempted to capture the non-linear spatio-temporal dependencies of crime. DeepCrime [23], a hierarchical recurrent framework with attention mechanism, considers

temporal correlation, its inter-relation with ubiquitous data and category dependencies for future crime prediction. However, DeepCrime does not consider spatial correlations of crimes. In [48], the authors applied ST-ResNet architecture [58] for crime intensity prediction while in [22], the authors developed MiST, a LSTM based neural network architecture with attention mechanism to model spatio-temporal and cross-categorical correlation for crime prediction. None of these models can capture dynamic spatial correlation and identify the impact of external features on crime predictions. Besides, these models are not interpretable. DeepCrime and MiST employ attention based RNNs which lack interpretability because of the recurrence on the hidden states generated by RNNs and their non-sparse attention weights for longer sequences. ST-ResNet uses deep residual units with hundreds and thousands of CNNs stacked altogether which makes it harder to interpret the model’s prediction.

2.2 Interpretable Models

The statistical and classic machine learning models have an advantage over deep learning models in terms of interpretability. However, they cannot model the complex non-linearity of space and time and thus lacks accuracy. On the other hand, though neural networks can capture the spatial-temporal non-linear relationship, they are not interpretable.

Attention-based models focus on the most relevant information while performing a certain task. These models have become very popular in image processing [1, 18, 34, 54] and natural language processing [2, 46], and health-care predictions [3, 10, 11, 33] for ensuring interpretability.

Attention-based models fall in the category of intrinsic models that have self-explanatory structure. The other category of interpretable models is post-hoc models, where a separate model is used for explanation. Examples of post-hoc models include LIME [38], SHAP [31], rule-based learning [43] and saliency visualizations [14].

2.3 Deep Learning for Spatio-temporal Prediction

Deep learning methods have become popular in recent years in the domain of spatial temporal prediction. A common approach is to use the convolution based architecture (CNN) [6, 8, 59] for finding the spatial correlation and the recurrent based architecture [13, 39] for finding the temporal correlation. In [20], the authors proposed a novel attention based spatial-temporal graph convolutional network model to solve the traffic flow forecasting problem. In [55], the authors used both CNN and attention-based LSTM to capture the dynamic spatio-temporal dependencies between regions for traffic prediction.

3 PROBLEM FORMULATION

In this section, we introduce some notations¹ and formulate crime prediction problem as a regression task. Table 1 summarizes the notations used in the paper.

Region. We model a city with an undirected graph $G = (V, E)$, where V represents a set of N regions $\{r_1, r_2, r_3, \dots, r_N\}$ and E represents a set of edges connecting them. In this study, a region denotes a community area: a pre-defined administrative boundary that serves various planning and statistical purposes. For a region r_i to be connected to region $r_{i'}$ they must share a common boundary.

Crime Occurrence. Let $x_{i,t}^k \in \mathbb{R}$ represent the number of crimes reported of category k (e.g. theft) at region r_i during t -th time step². If $\mathbf{x}_{i,t} = [x_{i,t}^1, x_{i,t}^2, x_{i,t}^3, \dots, x_{i,t}^K] \in \mathbb{R}^K$ denotes the reported crimes of all K categories at region r_i during t -th time step and $\mathbf{X}_t = (\mathbf{x}_{1,t}, \mathbf{x}_{2,t}, \mathbf{x}_{3,t}, \dots, \mathbf{x}_{N,t}) \in \mathbb{R}^{K \times N}$

¹Bold letters, e.g. A, a denote matrices and vectors respectively and small letters, e.g. a denote scalars

²We use time step and time interval synonymously.

denotes the reported crimes of all categories at all N regions during t -th time step, then the crime occurrences of the whole city for T time steps can be denoted as $\mathcal{X} = (X_1, X_2, \dots, X_T) \in \mathbb{R}^{K \times N \times T}$.

External Feature. We use POI information, traffic inflow and traffic outflow as external features for improving the model’s prediction accuracy. The external features of the city during T time steps are denoted as $\mathcal{F} = (F_1, F_2, \dots, F_T) \in \mathbb{R}^{J \times N \times T}$ for J external features, where $F_t = (f_{1,t}, f_{2,t}, f_{3,t}, \dots, f_{N,t}) \in \mathbb{R}^{J \times N}$ denotes the external features of the city during t -th time step, $f_{i,t} = [f_{i,t}^1, f_{i,t}^2, f_{i,t}^3, \dots, f_{i,t}^J] \in \mathbb{R}^J$ denotes the external features of a region r_i during time step t and $f_{i,t}^j \in \mathbb{R}$ denotes the j -th external feature of a region r_i during time step t .

Problem Definition. Given past crime occurrences \mathcal{X} and external features \mathcal{F} for last T time steps, predict $\hat{\mathbf{Y}}_{T+1}$, the crime occurrences of the city during $(T + 1)$ -th time step.

Table 1. Notations and their meanings

Notation	Symbol
N, T, K, J	Number of regions, time steps, crime categories, external features
\mathcal{N}_i	First-order neighbors of region r_i (including itself)
τ	Length of a time step
$x_{i,t}^k$	Crime occurrences of k -th category at region r_i during t -th time step
$\mathbf{x}_{i,t}$	Crime occurrences of all categories at region r_i during t -th time step
\mathbf{X}_t	Crime occurrences of all categories at all regions during t -th time step
$f_{i,t}^j$	j -th external feature of region r_i during t -th time interval
$\mathbf{f}_{i,t}$	All external features of region r_i during t -th time step
\mathbf{F}_t	All external features of all regions during t -th time step
$\hat{\mathbf{Y}}_{T+1}$	Predicted crime occurrences of all regions and categories of the city at $(T + 1)$ -th time step

4 MODEL DESCRIPTION

The key idea behind our model’s high prediction accuracy is that we exploit (i) hierarchical information of regions, (ii) external features, and (iii) short, long term crime patterns to capture the dynamic spatio-temporal dependencies while keeping the model’s architecture reasonably interpretable. Given the crime occurrences of category k at region r_i during time steps $[1..T]$, we find the crime embedding $\mathbf{c}_{i,t}^k$ and feature embedding $\mathbf{e}_{i,t}^k$ of r_i using hGAT and fGAT, respectively for each of these time step. These embedding are then fed to three SAB-LSTMs for capturing recent, daily and weekly trends which outputs the hidden states $\mathbf{h}_{T+1}^r, \mathbf{h}_{T+1}^d, \mathbf{h}_{T+1}^w$, respectively. After applying an attention mechanism on these hidden states, a context vector, \mathbf{c}_{T+1} is generated to predict the crime occurrence at $(T + 1)$ -th time step, $\hat{y}_{i,T+1}^k$. Figure 4 gives an overview of the model.

4.1 Spatial View

Convolutional neural networks (CNNs) [59] and its variants [55] have been applied to model spatial correlation between regions in spatio-temporal prediction. Though CNNs learn meaningful features on regular grid structured data, they do not perform well on irregular graph data because the number of nodes in a graph and their neighbor counts are variables. Urban crime data exhibit a clear graph structure considering the correlation between regions and other external features. Modeling them as grid structured data results in incomplete information and makes it hard to learn meaningful information. To address this issue, graph convolutional networks (GCNs) [28] have gained popularity in recent times. A GCNN learns a node’s embedding as an aggregation of its neighbor’s features and calculates their contribution with predefined Laplacian Matrix, which is the difference of the degree matrix and the adjacency matrix of the graph. Since the contributions of neighbor nodes are static, GCNN can not capture the dynamic spatial correlation between regions.

Based on these observations, we choose GAT as the base architecture to capture the spatial dependencies for crime prediction. Similar to GCNN, GAT learns a node’s embedding as an aggregation of its neighbor’s features but uses a self-attention mechanisms to learn their contributions instead. GAT does not require any costly matrix operation and knowledge about the graph structure upfront, which allows GAT to learn dynamic spatial correlation between regions.

We use two GAT variants: hGAT and fGAT to learn the crime and feature embedding of a target region as follows.

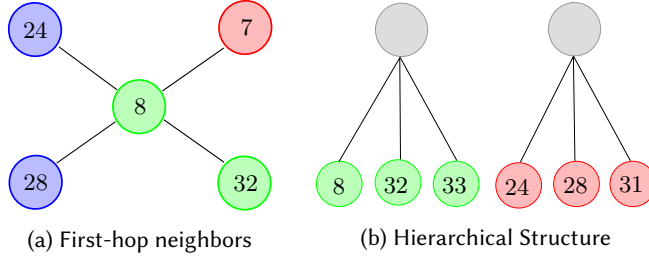


Fig. 3. Complex spatial interaction between regions

Crime Embedding. The city of Chicago is divided into 77 communities (regions) and the communities are grouped into 9 districts or sides forming a containment hierarchy. This hierarchical information shadows the information of similar crime distribution and urban dynamics. Hence, we propose *hGAT* to inject hierarchical information in GAT.

Figure 3 represents a scenario where the first-order neighbors of target region 8 are $\{7, 8, 24, 28, 32\}$ and target region 8 along with region 32 and 33 fall under the same side (represented as grey circles in Figure 3). It is expected that the target region 8 is influenced more by region 32 which is not only a first-hop neighbor but also falls under the same side, whereas regions 7, 24 or 28 do not. To be clear, we do not consider the influence of regions such as 33 that falls under the same side but is not a first-hop neighbor. We only want to amplify the signal from those regions which satisfy both conditions: falls under the same side and is a first-hop neighbor.

hGAT considers two sets of features for each node (r_i): (i) node level features: crime occurrences at community level during time step t : $x_{i,t}^k$, (ii) parent level features: crime occurrences at district/side level during time step t : $z_{i,t}^k$ as input to GAT and an additional attention layer to capture the similarity between nodes based on parent level features. Traditional GAT considers only node level features. Hence, it can not model hierarchical information into a node’s embedding.

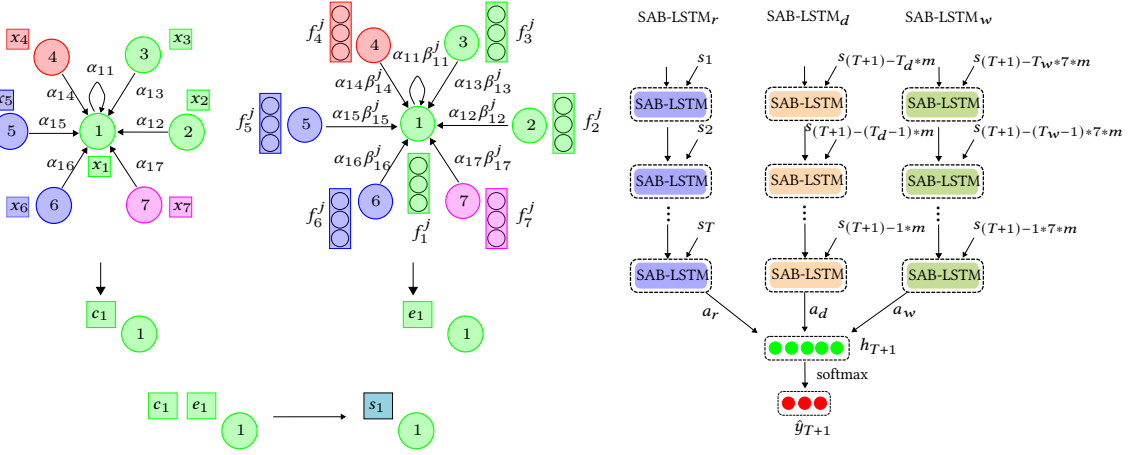


Fig. 4. Model Overview of AIST.

For hGAT, we use two transformation matrix, (i) $w_x \in \mathbb{R}^F$ to learn the similarities between a target region and its neighbor's node level features, and (ii) $w_z \in \mathbb{R}^F$ to learn similarities between their parent-level features. Based on these information two separate feed-forward attention layer computes two sets of pair-wise unnormalized attention scores between the target region and its first-hop neighbors: $e_{ii'}^c$ and $e_{ii'}^p$, respectively. For clarity, we omit the indices of crime categories (k) and time step (t).

$$e_{ii'}^c = \text{LeakyReLU}(a_x^T [w_x x_i \parallel w_x x_{i'}])$$

$$e_{ii'}^p = \text{LeakyReLU}(a_z^T [w_z z_i \parallel w_z z_{i'}])$$

We perform an element-wise addition to combine these two sets of unnormalized attention scores and apply softmax over them to generate final attention scores, where \mathcal{N}_i denotes first order neighbors including itself.

$$e_{ii'} = e_{ii'}^c + e_{ii'}^p$$

$$\alpha_{ii'} = \text{softmax}_{i'}(e_{ii'})$$

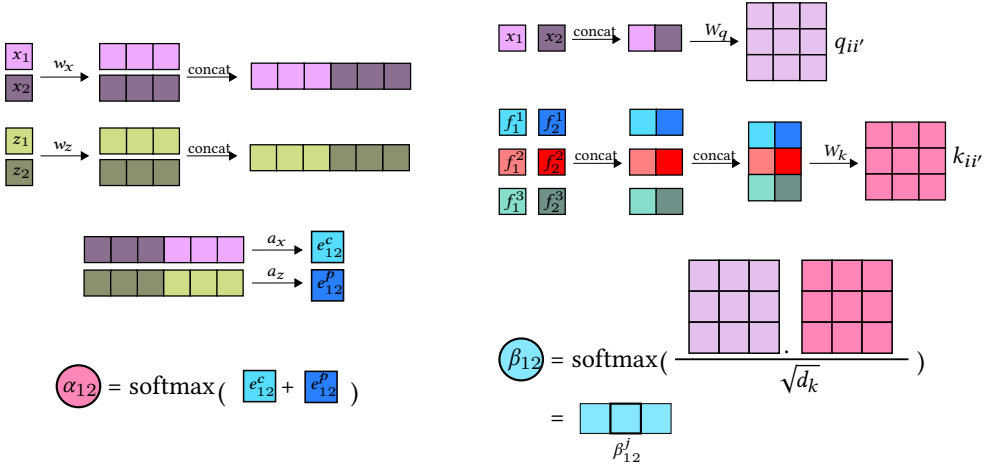
$$= \frac{\exp(e_{ii'})}{\sum_{i'' \in \mathcal{N}_i} \exp(e_{ii''})}$$

Finally, we use this combined attention score to update the crime embedding of target region r_i . Figure 5a gives an overview of the process of generating these attention scores.

$$c_{i,t}^k = \sigma \left(\sum_{i' \in \mathcal{N}_i} \alpha_{ii'} w_x x_{i',t}^k \right) \quad (1)$$

Feature Embedding. Besides historical crime observations, external features have been shown to be useful in crime prediction problems [23, 50, 60]. We propose *fGAT* that replaces additive self-attention mechanism with a novel scaled dot product self-attention mechanism [46] to learn category specific feature embedding of regions.

The feature embedding of a target region is formulated as an aggregation of its neighbors' features based on their possible influence on the crimes of the target region. The intuition behind



(a) Attention weights, $\alpha_{ii'}$ generation.

(b) Attention weights, $\beta_{ii'}^j$ generation

Fig. 5. Attention modules of AIST's spatial view.

finding a possible influential feature is - if two regions having similar features experience similar crime occurrences at a specific time step then the features might influence crimes or serve as proxies for crime prediction in addition to the crime occurrences.

We compute the query vector $q_{ii'}$ by multiplying the concatenated crime occurrences of a target region (r_i) and its neighbor region ($r_{i'}$) with weight matrix $W_q \in \mathbb{R}^{d_q \times 2}$ to learn their crime distribution similarities. For preparing the key vector $k_{ii'}^j$ for feature j , we multiply the concatenated features of r_i and $r_{i'}$ with weight matrix $W_k \in \mathbb{R}^{d_k \times 2}$ to learn their feature similarities. Here, d_q and d_k represents the dimension of the query and key vector, respectively.

$$q_{ii'} = W_q([x_{i,t}^k \parallel x_{i',t}^k])$$

$$k_{ii'}^j = W_k([f_{i,t}^j \parallel f_{i',t}^j])$$

Then, the attention weight of j -th feature of $r_{i'}$ is calculated using the dot-product attention mechanism.

$$\beta_{ii'}^j = \text{softmax}_j(\frac{q_{ii'} k_{ii'}^{jT}}{\sqrt{d_k}})$$

Once the attention weights of individual features are found, the feature embedding of r_i is formulated as follows. Figure 5b gives an overview of generating these attention weights.

$$e_{i,t}^k = \sigma \left(\sum_{i' \in N_i} \left(\alpha_{ii'} \sum_{j=1}^J \beta_{ii'}^j w_v f_{i',t}^j \right) \right) \quad (2)$$

Here $\beta_{ii'}^j w_v f_{i',t}^j$ represents the contribution of j -th feature of $r_{i'}$ on the feature embedding of r_i and $w_v \in \mathbb{R}^F$.

Finally, We concatenate the crime embedding, $c_{i,t}^k$ and feature embedding, $e_{i,t}^k$ to find spatial embedding $s_{i,t}^k$ of target region r_i at t -th time step for crime category k . This spatial embedding $s_{i,t}^k$ is fed as input to a SAB-LSTM cell for time step t as shown in Figure 4.

$$s_{i,t}^k = [c_{i,t}^k \parallel e_{i,t}^k]$$

4.2 Temporal View

LSTM and GRU are two popular recurrent neural networks (RNNs) that capture temporal correlations. However, besides being non-interpretable they suffer from vanishing gradient problem for long sequences. To address these issues, attention-based RNNs are proposed that use attention mechanism to focus on relevant hidden states. These attention weights are difficult to interpret because of the recurrence on the hidden states generated by LSTMs [11]. They are also not sparse enough to be meaningful for long sequence.

SAB-LSTM [27] back-propagates across only a selected small subset instead of all hidden states, which are selected using a sparse and hard attention mechanism. Thus it mitigates the gradient vanishing problem and is also interpretable. In this section, first we give a brief overview of a SAB-LSTM cell and then discuss how we apply them in predicting crimes.

At each time step t the underlying LSTM of SAB-LSTM takes the spatial embedding of region r_i , $s_{i,t}^k$ and the previous hidden state h_{t-1} as inputs for crime category k . It produces a new cell state c_t along with a provisional hidden state \hat{h}_t .

$$\hat{h}_t, c_t = \text{LSTM}(s_{i,t}^k, h_{t-1})$$

The provisional hidden state, \hat{h}_t is concatenated with all the vectors stored in memory $\mathcal{M} = [h_1^{mem}, h_2^{mem}, \dots, h_{|\mathcal{M}|}^{mem}]$ and passed through a feed-forward neural network to generate unnormalized attention weights (e_m) for each vector stored in the memory. Memory \mathcal{M} contains a set of hidden states selected arbitrarily (after each k_{att} time step) for comparison with the generated provisional hidden state.

$$e_m = W_m \tanh(\hat{h}_t \parallel h_m^{mem})$$

Then, SAB-LSTM subtracts the $(k_{top} + 1)$ -th highest attention score from all the attention scores and use normalization to generate k_{top} sparse attention weights to select only k_{top} memory cells.

$$\alpha_m = \frac{e_m - e_{k_{top}+1}}{\sum_{m'' \in \mathcal{M}} (e_{m''} - e_{k_{top}+1})}$$

Once the attention weights (α_m) are obtained, it calculates a summary vector sum_t by summing over the k_{top} memories. This summary vector is then concatenated to the previously generated hidden provisional state \hat{h}_t to get the final hidden state, h_t .

$$\begin{aligned} \text{sum}_t &= \sum_{m \in \mathcal{M}} \alpha_m h_m^{mem} \\ h_t &= \hat{h}_t + \text{sum}_t \end{aligned}$$

The hidden state generated at time step t has two contributing factors. First, the provisional hidden vector (\hat{h}_t) which is the output of a traditional LSTM at time t and non-interpretable. Second, the summary vector sum_t which is the summation of dynamic, sparse hidden states aligned with current state and interpretable. For crime prediction task we omit the first contributing factor and only use the summary vector sum_t as our output hidden state h_t . Even though the accuracy is slightly compromised but this makes SAB-LSTM more interpretable.

$$h_t = \text{sum}_t = \sum_{m \in \mathcal{M}} \alpha_m h_m^{\text{mem}} \quad (3)$$

We use three SAB-LSTMs for our crime prediction task. SAB-LSTM_r captures recent crime trends based on a target region’s spatial embedding during past T time steps. SAB-LSTM_d captures daily trends based on spatial embedding at the same time step as the predicted time step but on previous days. Finally, SAB-LSTM_w captures weekly trends based on the the spatial embedding at the same time step as the predicted time step but on previous weeks. We formulate them as follows. For simplicity of representation, we omit region-index i and crime category-index k .

$$\begin{aligned} h_{T+1}^r &= \text{SAB-LSTM}_r(s_t) \\ h_{T+1}^d &= \text{SAB-LSTM}_d(s_{(T+1)-t_d*m}) \\ h_{T+1}^w &= \text{SAB-LSTM}_w(s_{(T+1)-t_w*7*m}) \end{aligned}$$

Here, $t = [1..T]$, $t_d = [1..T_d]$, $t_w = [1..T_w]$, $m = 24/\tau$, $T_d = T/m$, $T_w = T/(m * 7)$, $\tau =$ length of each time step. $h_{T+1}^r, h_{T+1}^d, h_{T+1}^w \in \mathbb{R}^H$, $H =$ hidden state dimension.

After calculating the final hidden states of all three SAB-LSTMs we use location-based attention mechanism [32] to capture the contribution (α_a) of the recent, daily and weekly trends. Then, a context vector is calculated using the generated attention weights. Here, $W_h \in \mathbb{R}^{H \times A}$, $b_h \in \mathbb{R}^A$ are learnable parameters, $A =$ attention dimension and $a = \{r, d, w\}$.

$$\begin{aligned} \alpha_a &= \text{softmax}_a(\tanh(W_h^T h_{T+1}^a + b_h)) \\ c_{i,T+1}^k &= \sum_a \alpha_a h_{T+1}^a \end{aligned} \quad (4)$$

Finally, the context vector is fed to a fully connected layer for predicting the crime occurrence at time step $(T + 1)$ for region r_i and crime category k where, $w \in \mathbb{R}^H$, $b \in \mathbb{R}$ are learnable parameters. We add the previously omitted region-index i and crime category-index k below.

$$\hat{y}_{i,T+1}^k = \tanh(w c_{i,T+1}^k + b) \quad (5)$$

5 EXPERIMENT

5.1 Experimental Settings

5.1.1 Data-sets. We evaluate our model on publicly available 2019 Chicago crime data [12], following the state-of the-art [50, 51]. Chicago is one of the most violent cities of United States and the crime concentration of Chicago is very diverse; it has both some of the safest and some of the most crime prone neighborhoods. We did not find any other city for which both crime and external feature data are available. We use 2019 Chicago taxi trip data [45] and POI information as external features. We collect POI information from FourSquare API while Chicago crime and taxi data are publicly available.

- **Chicago-Crime** (2019). We select 152,720 crime records of four crime categories: theft, criminal damage, battery, narcotics from 1/1/2019 to 31/12/2019 and extract these information of each record: timestamp, primary category of crime, community area where it occurred.
- **Chicago-POI** We select 89,324 POIs of 10 categories: food, residence, travel, arts & entertainment, outdoors & recreation, education, nightlife, professional, shops and event.
- **Chicago-Taxi** (2019). We select 29,110,097 taxi trips from 1/1/2019 to 31/12/2019 and extract these information of each record: pickup timestamp, drop-off timestamp, pickup community area, drop-off community area.

5.1.2 Data Preprocessing. We consider Chicago crime data of first 8 months as training set and the remaining of the last 4 months as test set, 10% of which is selected as validation set. We use taxi inflow (F1), outflow (F2) and POI category: food (F3), residence (F4), travel (F5), arts & entertainment (F6), outdoors & recreation (F7), education (F8), nightlife (F9), professional (F10), shops (F11) and event (F12) as external features. The time step is set to 4 hours. We use Min-Max normalization to scale the crime events to $[-1, 1]$ and later denormalize the prediction to get the actual number of crime events. Following [51], we do not scale the external features.

5.1.3 Parameter settings. We train our model using Adam optimizer with batch size = 42 and initial learning rate = 0.001.

hGAT & fGAT settings. Both hGAT and fGAT are single layer GATs consisting of single attention head for computational efficiency. We set dimensions (F, F') of hGAT's both transformation matrices to 8. For fGAT, we set $d_q = 40, d_k = 40$, and $d_v = 8$. Dropout with $p = 0.5$ is applied to unnormalized node-level (e_{iv}^c), unnormalized parent-level (e_{iv}^p), normalized combined attention weights ($\alpha_{ii'}$) in hGAT, and dropout with $p = 0.5$ is applied to normalized dot-product attention weights ($\beta_{ii'^j}$) in fGAT.

SAB-LSTM settings. All 3 SAB-LSTMs are single layered with hidden dimension $H = 40$. For $SAB-LSTM_r$ and $SAB-LSTM_d$, we set $k_{att} = 5, k_{top} = 5, trunc_{length} = 5$. For $SAB-LSTM_w$ we set $k_{att} = 1, k_{top} = 5, trunc_{length} = 1$. Dropout with $p = 0.2$ is applied to each output of 3 SAB-LSTMs. Finally, we set the attention dimension of location based attention as $A = 30$.

5.1.4 Evaluation Criteria. We use mean average error (MAE) and mean square error (MSE) to evaluate AIST predictions. Here, n represents the number of predictions, y_i represents the predicted result and \hat{y}_i represents the ground truth.

$$MAE = \frac{1}{n} \sum_{i=1}^n |y_i - \hat{y}_i| \quad MSE = \frac{1}{n} \sum_{i=1}^n (y_i - \hat{y}_i)^2$$

We also use Total Variation Distance (TVD) for comparing prediction scores and Jensen-Shannon Divergence (JSD) for comparing attention weight distributions to evaluate interpretations of AIST, where $\alpha = \frac{\alpha_1 + \alpha_1}{2}$ and $KL(p||q)$ calculates the Kullback–Leibler divergence between probability distributions p and q .

$$TVD = \frac{1}{2} \sum_{i=1}^{|y|} (|\hat{y}_{1i} - \hat{y}_{2i}|)$$

$$JSD(\alpha_1, \alpha_2) = \frac{1}{2} KL[\alpha_1 || \alpha] + \frac{1}{2} KL[\alpha_2 || \alpha]$$

5.1.5 Baselines. We compare AIST with the following baselines:

- ARIMA. The most general case of models for predicting time series combining moving average and auto-regression.
- DTR. A decision tree algorithm for regression that chooses the best random split while separating samples.
- Att-RNN. It uses attention mechanism with RNN to capture temporal correlation.
- DeepCrime [23]. A hierarchical recurrent framework that encodes temporal correlation and inter-dependencies between crimes and urban anomalies.
- MiST [22]. It uses multiple LSTMs to encode spatial, temporal and categorical view of crime.

Table 2. Comparison of AIST with baselines on Chicago Crime Data (2019)

Crime Category	Criteria	ARIMA	DTR	Att-RNN	DeepCrime	MiST	AIST
Theft (C1)	MAE	1.2010	1.1943	1.0419	1.0022	1.0241	0.8747
	MSE	2.8492	3.3275	2.5443	2.6279	2.5153	1.6986
Criminal Damage (C2)	MAE	0.5863	0.5590	0.4096	0.3727	0.3727	0.3615
	MSE	0.7238	0.8123	0.4427	0.4751	0.4836	0.4837
Battery (C3)	MAE	0.8840	0.8983	0.7377	0.7271	0.7365	0.6910
	MSE	1.4242	1.9336	1.0665	1.0567	1.0345	0.9568
Narcotics (C4)	MAE	0.5705	0.4901	0.4128	0.3702	0.3701	0.3399
	MSE	0.7928	0.8522	0.6380	0.6394	0.6495	0.5609

5.2 Prediction Performance

5.2.1 Comparison with baselines. The performance of the baselines and AIST is shown in Table 2. AIST outperforms all baselines by achieving the lowest MAE and MSE across all crime categories except Criminal Damage on MSE, which may be due to the fact that this crime category lacks periodicity and spatial correlation. As a result, Att-RNN that considers only temporal correlation is able to perform better than AIST. Interpretable models (ARIMA, DTR) can not model the non-linear spatial and temporal dependencies and shows poor performance. Att-RNNs capture the temporal dynamics but do not consider the spatial correlation or external features. Deep learning NNs (DeepCrime, MiST) perform better than interpretable models and Att-RNN because of their ability to model spatial or temporal or both correlation. However, they do not consider dynamic spatio-temporal correlation and can not utilize external features properly. AIST can model non-linear dynamic spatial correlation, crime periodicity and utilize the external features.

5.2.2 Effectiveness of different components of AIST. We run experiments on 4 models that differ in spatial view. The spatial structure of these models constitute of GAT, hGAT, hGAT concatenated with external features and lastly hGAT along with fGAT (actual AIST model). Fig 6 shows that hGAT outperforms GAT because hierarchical information are important for learning node embedding. Traditional feature concatenation technique seems to deteriorate the performance of hGAT on

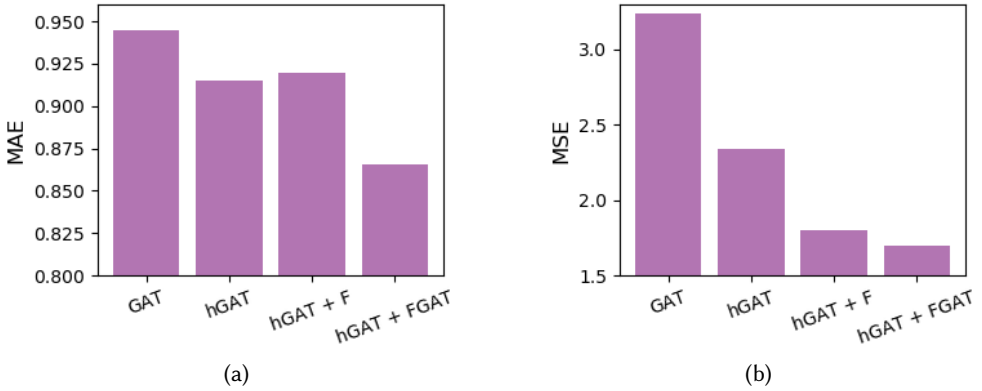


Fig. 6. Effectiveness of different components

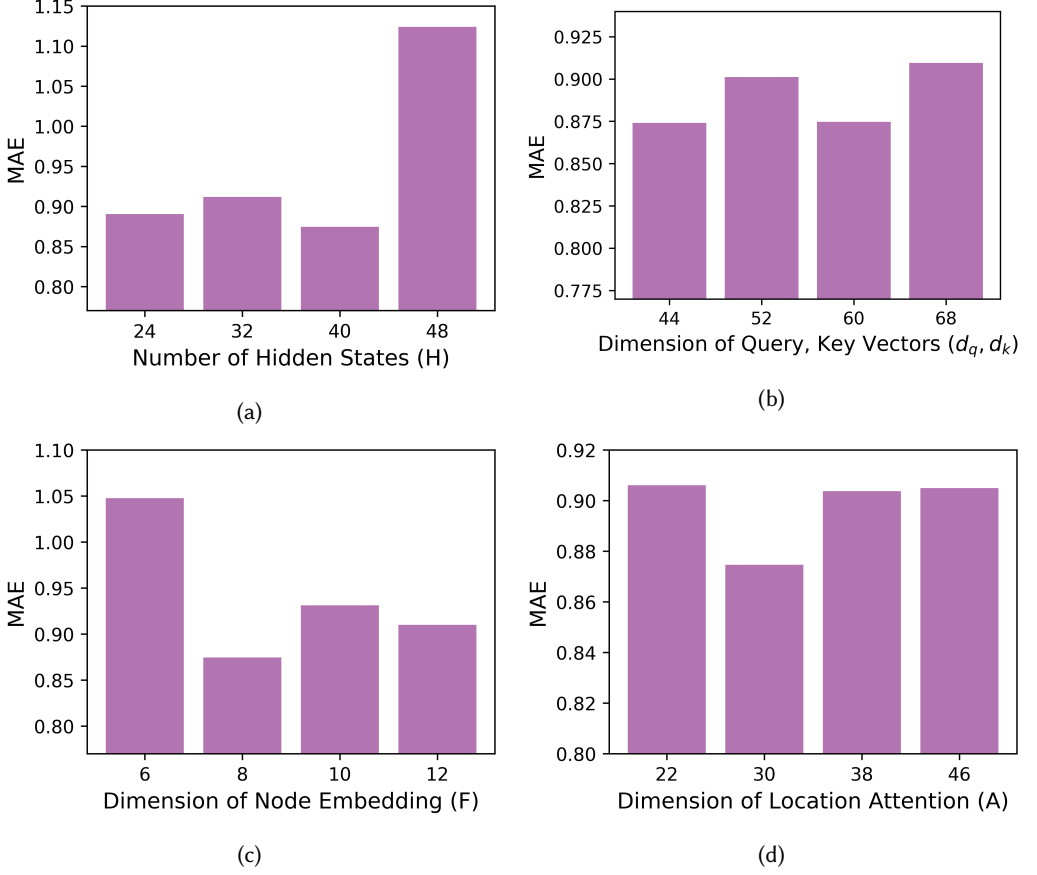


Fig. 7. Impact of parameters in prediction.

MAE. Above all, hGAT along with fGAT outperforms all other variants asserting the fact that fGAT learns better crime specific node embedding.

5.2.3 Parameter sensitivity. Figure 7 shows that AIST is sensitive to a node’s embedding size and the number of hidden states of SAB-LSTMs. This is because limited information about the nodes makes it harder to train the SAB-LSTMs and hence they easily overfit. A large embedding size is required for more reliable representation. Chicago crime dataset has 2069 timestamps and 77 nodes (regions), which makes it easier to overfit for large hidden dimension of SAB-LSTMs. Other than these two, the dimensions of location based attention (A), query (d_Q) and key vectors (d_k) are less sensitive to changes.

5.3 Evaluation of Interpretability

The notion of interpretability mainly comes down to two points: i) plausibility: how understandable it is to humans, and ii) faithfulness: how accurately it refers to the true reasoning process of a model.

Besides human evaluations [17, 26, 36], explanations that align directly with the input have been considered as plausible explanations [29]. Attentions are plausible explanations because they

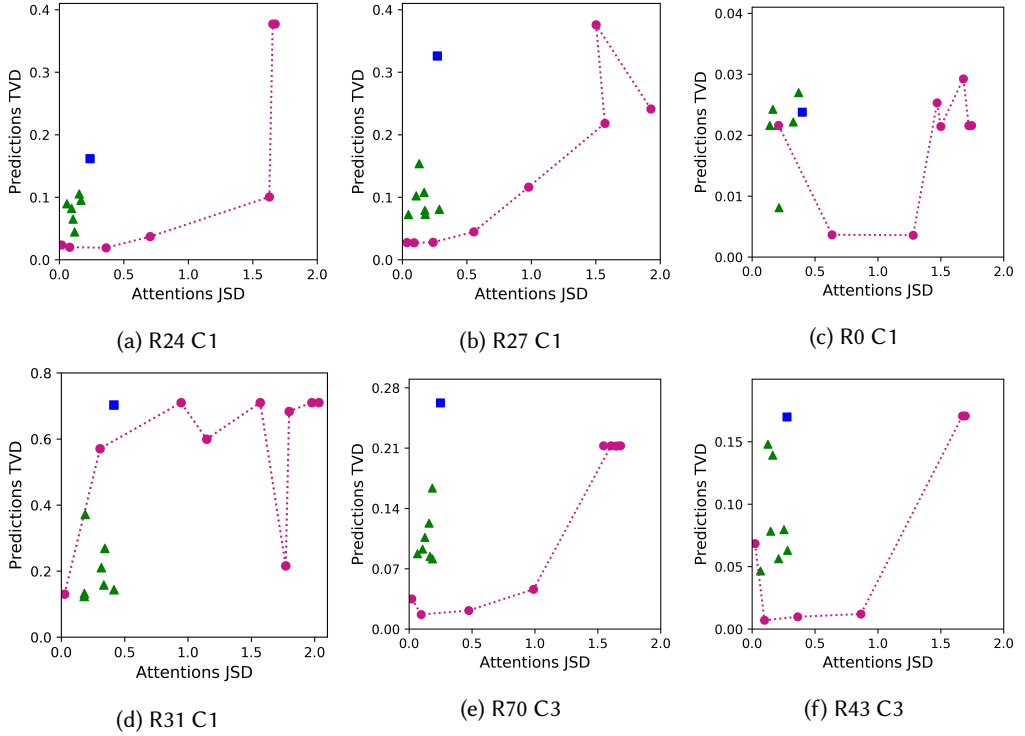


Fig. 8. Evaluation of interpretability (Averaged per-instance test set JSD and TVD from base model for each model variant. JSD is bounded at ~ 2.07 ; \blacktriangle : random seed; \blacksquare : uniform weights; dotted line: our adversarial setup as λ is varied)

assign importance weights to the inputs while making a prediction [52]. Since AIST interprets the importance of different regions, features, time steps and trends on the crime prediction based on four attention modules, the interpretation of AIST is *plausible*.

A recent study [52] shows the conditions under which attentions can be regarded as faithful explanations, and nullifies the claim [25, 42] that criticizes attention as a form of faithful explanation due to its weak correlation with other feature importance metrics and the existence of alternate adversarial attention weights. Specifically, [52] proposes a series of extensive experiments based on dataset and model properties: i) train on uniform attention weights: the attention distribution is frozen to uniform weights to validate whether the attention is actually necessary for a better performance, ii) calibration of variance: the model is trained with different initializing seeds to generate base variance for attention distributions, iii) train an MLP (multilayer perceptron): the LSTM cells are replaced by MLP and are trained separately and iv) train an adversary: the model is trained to provide similar predictions as the base model while keeping the attention distributions distant from the actual ones for ascertaining exclusivity. We evaluate the attention weights generated by AIST by performing these experiments (except iii since the attention modules used in AIST are either feed-forward neural networks or sparse which do not comply with the experimental settings) to validate their *faithfulness*.

Since the faithfulness varies across model, tasks and input space, both [24, 52] emphasize that the faithfulness should be evaluated in grayscale instead of a binary term, i.e., faithful or not faithful.

Following [24, 52], we consider the degree of faithfulness as it allows to identify the interpretation that is sufficiently faithful to be useful in practice.

Our process to generate the adversarial attention weights to establish the exclusivity, hence the faithfulness of the model is as follows. We train an adversarial model (\mathcal{M}_{adv}) with the objective of minimizing the prediction differences from our AIST model (\mathcal{M}_{AIST}) along with a divergent attention distribution for an instance i .

$$\mathcal{L}(\mathcal{M}_{AIST}, \mathcal{M}_{adv}) = \text{TVD}(\hat{y}_{AIST}^{(i)}, \hat{y}_{adv}^{(i)}) - \lambda \text{KL}(\alpha_{AIST}^{(i)}, \alpha_{adv}^{(i)})$$

Here, λ is a hyperparameter that controls the tradeoff between TVD and JSD, where TVD is the levels of prediction variance and JSD (Jensen-Shannon Divergence) quantifies the difference between two attention distributions. In Figure 8, we present the TVD between the predictions of the adversarial and AIST model against the increasing JSD between their attention distributions for a selected number of regions on specific crime categories. We believe the graphs in Figure 8 to be representative of all 4 crime categories across 77 regions as they show all of the possible three cases: not faithful, moderately faithful and concretely faithful. Fast increase in the prediction difference concurs that the attention scores are not easily manipulable and exclusive. Hence, they can be used as faithful explanations. We also include the scores of uniform model variant (■) and random seed initialization (▲) in these TVD vs JSD graphs. Figure 8a, 8b, 8d, 8e, 8f establish attentions as faithful explanations for the specified regions and crime categories as the increase in JSD comes at a high price of the increased TVD (at different rates). However, Figure 8c shows an example where the attention distributions generated by AIST can not be deemed faithful as it is easy to manipulate the attentions without losing much of the prediction performance. We include the predictions of the best adversarial models with instance-average JSD > 1 in Table 3.

Table 3 shows the superiority of the base model (AIST) across all four crime categories over its uniform variant and adversarial models. Substantial increase of MAE scores of the uniform model suggests that attention is indeed a necessary component for better performance in the crime prediction. Similarly, a higher MAE score of the adversarial models ascertain the exclusivity of the predictions generated by AIST model.

Table 3. Comparison of AIST with its uniform variant and adversarial models on MAE

Crime Category	Uniform	Base Model	Adversarial
Theft (C1)	0.9776	0.8747	1.1807
Criminal Damage (C2)	0.3738	0.3615	0.3734
Battery (C3)	0.7206	0.6910	0.8029
Narcotics (C4)	0.3634	0.3399	0.5537

5.4 Case Study

We select three communities for exploration: (i) R8 (Near North Side): situated in downtown Central Chicago and experiences high crime distribution, (ii) R25 (Austin): situated on the Western side of Chicago and is not as busy as R8, but has a high crime distribution and (iii) R72 (Beverly): located in Southern Chicago and is a quiet residential community with low crime rate. For each community, we randomly select 200 samples from test set and present the contribution of neighbor regions, POI and taxi flow features, trends and important time steps as a heat map in Figure 9. We denote crimes category Theft, Criminal Damage, Battery and Narcotics with C1, C2, C3 and C4, respectively.

From Equation 1, the contribution coefficient of the crime occurrences of region $r'_i \in \mathcal{N}_i$ to the crime embedding of target region r_i during time step t can be calculated as, $\phi(c_{i,t}^k, x_{i',t}^k) = \alpha_{i'w_x} x_{i',t}^k$.

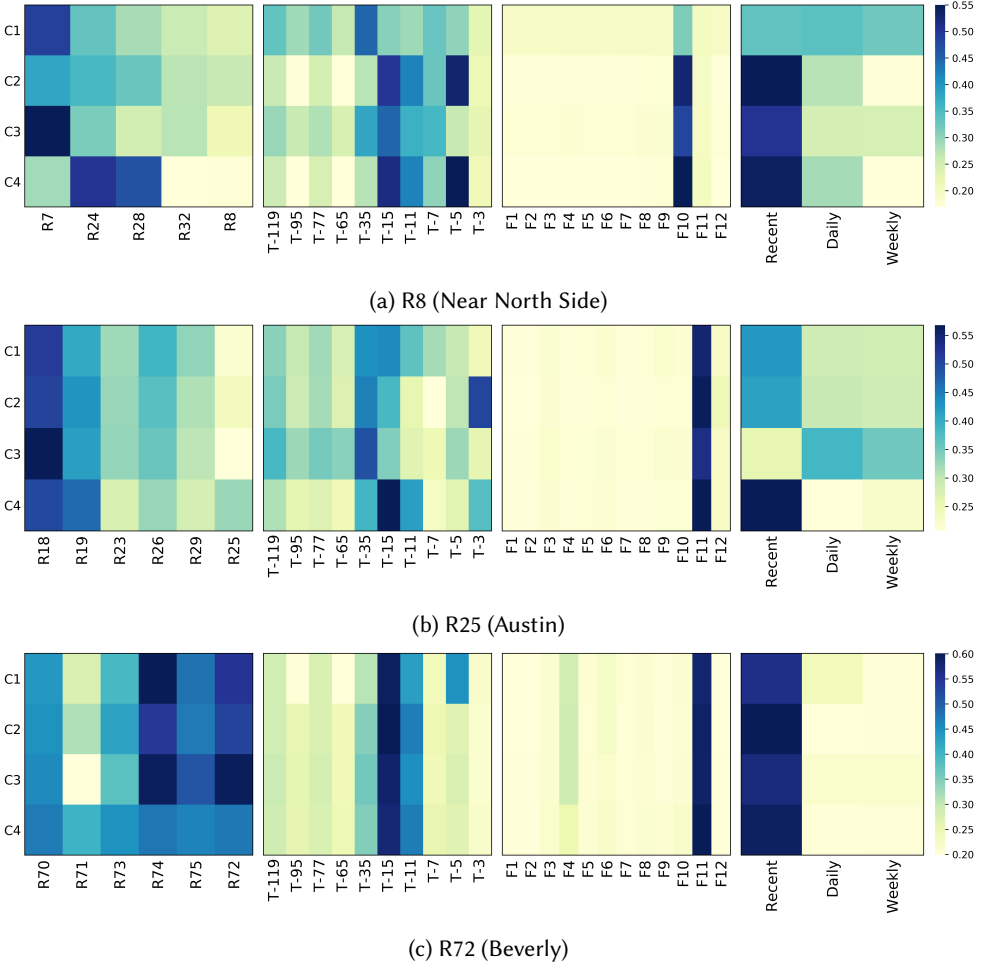


Fig. 9. Case analysis of Region 8, 25 and 72

From Equation 2, the contribution coefficient of feature j on target region can be calculated as $\phi(e_{i,t}^k, f_t^j) = \beta_{i,t}^j \sum_{i' \in N_i} \alpha_{i,i'} w_v f_{i',t}^j$. Similarly, $\phi(\hat{y}_{i,T+1}^k, h_{T+1}^a) = \alpha_a w_h^a$ denotes the contribution coefficient of recent, daily and periodic trends (Equations 4, 5).

For R8, professional POIs (F10) made the highest contribution. R8 is a business region with thousands of jobs and has a large number of professional POIs. Thus it is expected that those POIs have large impact on it's crime embedding. On the other hand, R25 and R72 are residential regions. POI Shop (F11) contributed most for R25 and R72. Besides F11, Residence (F4) POIs also contributed for R72 for all categories except C4. Hence, our model learns both region and category specific influential features. An interesting observation for R8 is that though R8 has a large number of Food and Shop POIs, their contribution is almost none which signifies the quality of our model's prediction.

C1 shows strong long term temporal correlation for R8, whereas none of the crime category shows long term temporal correlation for R72 as the crime number for R72 is low. C3 in R25 shows

a strong periodic correlation and unlike R8 and R72, it does not depend on recent crimes. C4 hardly present any long term correlation, which is intuitive. C2 shows daily periodicity in R8 and R25.

R7 and R24 have the most similar crime distribution as R8. However, these similarities vary with crime categories, e.g. for C1 and C3, R7 is given more attention whereas for C4, the attention shifts to R24 and R28. This is because both R24 and R28 experience large number of C4 crimes and have greater influence than R7. For R25, R18 is the most influential region across all crime categories. Unlike R8, the contribution of its neighboring regions are almost same except for R23 which is given less importance compared to other neighbors. The fact that R23 shares its boundary with different regions of different districts/sides makes their crime distribution less similar. R72 gives equal importance to each of its neighbors except R71. R71 has a higher number of crime occurrences than R72 and their crime distribution is quite different for all crime categories except C4. Thus, our model is able to capture diverse spatial correlation.

6 CONCLUSION

We propose AIST, a novel interpretable deep learning framework for crime prediction. AIST captures the dynamic spatio-temporal correlations based on the past crime occurrences, external features (e.g., traffic flow and POI information) and the recent and periodic crime trends. We develop two novel variants of GAT, *hGAT* and *fGAT* that allows AIST to improve prediction accuracy and provide the insights behind a prediction. Experiments and case studies on real-world Chicago crime data show that AIST outperforms the baseline models in terms of prediction accuracy and we can exploit attention weights associated with different parts of the model to interpret its prediction. On average, AIST shows a decrease of 8.3% on MAE and 20.98% on MSE over the state-of-the-art.

Though we evaluate AIST for the crime prediction problem, AIST has the ability to learn an arbitrary function over the spatio-temporal-semantic space and can be adapted for any other spatio-temporal problem (e.g. traffic, citywide passenger demand, taxi demand prediction) that can benefit from incorporating semantically relevant information and knowing the interpretation of the prediction.

REFERENCES

- [1] Jimmy Ba, Volodymyr Mnih, and Koray Kavukcuoglu. 2015. Multiple Object Recognition with Visual Attention. In *ICLR*.
- [2] Dzmitry Bahdanau, Kyunghyun Cho, and Yoshua Bengio. 2015. Neural Machine Translation by Jointly Learning to Align and Translate. In *ICLR*.
- [3] Tian Bai, Shanshan Zhang, Brian L. Egleston, and Slobodan Vucetic. 2018. Interpretable Representation Learning for Healthcare via Capturing Disease Progression through Time. In *SIGKDD*. ACM, 43–51.
- [4] Anna L. Buczak and Christopher M. Gifford. 2010. Fuzzy Association Rule Mining for Community Crime Pattern Discovery. In *ACM SIGKDD Workshop on Intelligence and Security Informatics*. Association for Computing Machinery.
- [5] Spencer Chainey, Lisa Tompson, and Sebastian Uhlig. 2008. The Utility of Hotspot Mapping for Predicting Spatial Patterns of Crime. *Security Journal* 21 (2008), 4–28.
- [6] Cen Chen, Kenli Li, Sin G. Teo, Guizi Chen, Xiaofeng Zou, Xulei Yang, Ramaseshan C. Vijay, Jiashi Feng, and Zeng Zeng. 2018. Exploiting Spatio-Temporal Correlations with Multiple 3D Convolutional Neural Networks for Citywide Vehicle Flow Prediction. In *ICDM*. IEEE Computer Society, 893–898.
- [7] Chaofan Chen, Oscar Li, Daniel Tao, Alina Barnett, Cynthia Rudin, and Jonathan Su. 2019. This Looks Like That: Deep Learning for Interpretable Image Recognition. In *NeurIPS*. 8928–8939.
- [8] Meng Chen, Xiaohui Yu, and Yang Liu. 2018. PCNN: Deep Convolutional Networks for Short-Term Traffic Congestion Prediction. *IEEE Trans. Intell. Transp. Syst.* 19, 11 (2018), 3550–3559.
- [9] P. Chen, H. Yuan, and X. Shu. 2008. Forecasting Crime Using the ARIMA Model. In *FSKD*. 627–630.
- [10] Edward Choi, Mohammad Taha Bahadori, Le Song, Walter F. Stewart, and Jimeng Sun. 2017. GRAM: Graph-based Attention Model for Healthcare Representation Learning. In *SIGKDD*. ACM, 787–795.
- [11] Edward Choi, Mohammad Taha Bahadori, Jimeng Sun, Joshua Kulas, Andy Schuetz, and Walter F. Stewart. 2016. RETAIN: An Interpretable Predictive Model for Healthcare using Reverse Time Attention Mechanism. In *NeurIPS*.

3504–3512.

- [12] Chicago Crimes. 2019. City of Chicago Data Portal. <https://data.cityofchicago.org/Public-Safety/Crimes-2019/w98m-zvie>.
- [13] Zhiyong Cui, Ruimin Ke, and Yinhai Wang. 2016. Deep Stacked Bidirectional and Unidirectional LSTM Recurrent Neural Network for Network-wide Traffic Speed Prediction. (2016).
- [14] Piotr Dabkowski and Yarin Gal. 2017. Real Time Image Saliency for Black Box Classifiers. In *NeurIPS*. 6967–6976.
- [15] Jose Florencio de Queiroz Neto, Emanuele Marques dos Santos, and Creto Augusto Vidal. 2016. MSKDE - Using Marching Squares to Quickly Make High Quality Crime Hotspot Maps. In *SIBGRAPI*. IEEE Computer Society, 305–312.
- [16] John Eck, Spencer Chainey, James Cameron, and Ronald Wilson. 2005. Mapping crime: Understanding hotspots. (2005).
- [17] Upol Ehsan, Pradyumna Tambwekar, Larry Chan, Brent Harrison, and Mark O. Riedl. 2019. Automated rationale generation: a technique for explainable AI and its effects on human perceptions. In *IUI*. ACM, 263–274.
- [18] Jianlong Fu, Heliang Zheng, and Tao Mei. 2017. Look Closer to See Better: Recurrent Attention Convolutional Neural Network for Fine-Grained Image Recognition. In *CVPR*. IEEE Computer Society, 4476–4484.
- [19] Matthew S. Gerber. 2014. Predicting crime using Twitter and kernel density estimation. *Decis. Support Syst.* 61 (2014), 115–125.
- [20] Shengnan Guo, Youfang Lin, Ning Feng, Chao Song, and Huaiyu Wan. 2019. Attention Based Spatial-Temporal Graph Convolutional Networks for Traffic Flow Forecasting. In *AAAI*. 922–929.
- [21] Timothy Hart and Paul Zandbergen. 2014. Kernel density estimation and hotspot mapping: Examining the influence of interpolation method, grid cell size, and bandwidth on crime forecasting. *Policing: An International Journal of Police Strategies and Management* 37 (05 2014).
- [22] Chao Huang, Chuxu Zhang, Jiashu Zhao, Xian Wu, Nitesh V. Chawla, and Dawei Yin. 2019. MiST: A Multiview and Multimodal Spatial-Temporal Learning Framework for Citywide Abnormal Event Forecasting. In *WWW*. ACM, 717–728.
- [23] Chao Huang, Junbo Zhang, Yu Zheng, and Nitesh V. Chawla. 2018. DeepCrime: Attentive Hierarchical Recurrent Networks for Crime Prediction. In *CIKM*. ACM, 1423–1432.
- [24] Alon Jacovi and Yoav Goldberg. 2020. Towards Faithfully Interpretable NLP Systems: How Should We Define and Evaluate Faithfulness?. In *ACL*. Association for Computational Linguistics, 4198–4205.
- [25] Sarthak Jain and Byron C. Wallace. 2019. Attention is not Explanation. In *NAACL-HLT*. Association for Computational Linguistics, 3543–3556.
- [26] Harmanpreet Kaur, Harsha Nori, Samuel Jenkins, Rich Caruana, Hanna M. Wallach, and Jennifer Wortman Vaughan. 2020. Interpreting Interpretability: Understanding Data Scientists’ Use of Interpretability Tools for Machine Learning. In *CHI*. ACM, 1–14.
- [27] Nan Rosemary Ke, Anirudh Goyal, Olexa Bilaniuk, Jonathan Binas, Michael C. Mozer, Chris Pal, and Yoshua Bengio. 2018. Sparse Attentive Backtracking: Temporal Credit Assignment Through Reminding. In *NeurIPS*. 7651–7662.
- [28] Thomas N. Kipf and Max Welling. 2017. Semi-Supervised Classification with Graph Convolutional Networks. In *ICLR*. OpenReview.net.
- [29] Tao Lei, Regina Barzilay, and Tommi S. Jaakkola. 2016. Rationalizing Neural Predictions. In *EMNLP*. The Association for Computational Linguistics, 107–117.
- [30] Youru Li, Zhenfeng Zhu, Deqiang Kong, Meixiang Xu, and Yao Zhao. 2019. Learning Heterogeneous Spatial-Temporal Representation for Bike-Sharing Demand Prediction. In *AAAI*. AAAI Press, 1004–1011.
- [31] Scott M. Lundberg and Su-In Lee. 2017. A Unified Approach to Interpreting Model Predictions. In *NeurIPS*. 4765–4774.
- [32] Thang Luong, Hieu Pham, and Christopher D. Manning. 2015. Effective Approaches to Attention-based Neural Machine Translation. In *EMNLP*. ACL, 1412–1421.
- [33] Fenglong Ma, Radha Chitta, Jing Zhou, Quanzeng You, Tong Sun, and Jing Gao. 2017. Dipole: Diagnosis Prediction in Healthcare via Attention-based Bidirectional Recurrent Neural Networks. In *SIGKDD*. ACM, 1903–1911.
- [34] Volodymyr Mnih, Nicolas Heess, Alex Graves, and Koray Kavukcuoglu. 2014. Recurrent Models of Visual Attention. In *NeurIPS*. 2204–2212.
- [35] G. O. Mohler, M. B. Short, P. J. Brantingham, F. P. Schoenberg, and G. E. Tita. 2011. Self-Exciting Point Process Modeling of Crime. *J. Amer. Statist. Assoc.* 106, 493 (2011), 100–108.
- [36] James Mullenbach, Sarah Wiegrefe, Jon Duke, Jimeng Sun, and Jacob Eisenstein. 2018. Explainable Prediction of Medical Codes from Clinical Text. In *NAACL-HLT*. Association for Computational Linguistics, 1101–1111.
- [37] Tomoki Nakaya and Keiji Yano. 2010. Visualising Crime Clusters in a Space-time Cube: An Exploratory Data-analysis Approach Using Space-time Kernel Density Estimation and Scan Statistics. *Trans. GIS* 14, 3 (2010), 223–239.
- [38] Marco Túlio Ribeiro, Sameer Singh, and Carlos Guestrin. 2016. “Why Should I Trust You?”: Explaining the Predictions of Any Classifier. In *SIGKDD*. ACM, 1135–1144.

- [39] Yuecheng Rong, Zhimian Xu, Ruibo Yan, and Xu Ma. 2018. Du-Parking: Spatio-Temporal Big Data Tells You Realtime Parking Availability. In *SIGKDD*. ACM, 646–654.
- [40] Cynthia Rudin. 2019. Stop explaining black box machine learning models for high stakes decisions and use interpretable models instead. *Nature Machine Intelligence* 1, 5 (2019), 206–215.
- [41] Shakila Khan Rumi, Phillip Luong, and Flora D. Salim. 2019. Crime Rate Prediction with Region Risk and Movement Patterns. *CoRR* abs/1908.02570 (2019).
- [42] Sofia Serrano and Noah A. Smith. 2019. Is Attention Interpretable?. In *ACL*. Association for Computational Linguistics, 2931–2951.
- [43] Guolong Su, Dennis Wei, Kush R. Varshney, and Dmitry M. Malioutov. 2016. Interpretable Two-level Boolean Rule Learning for Classification. *CoRR* abs/1606.05798 (2016).
- [44] Jameson L. Toole, Nathan Eagle, and Joshua B. Plotkin. 2011. Spatiotemporal correlations in criminal offense records. *TIST* 2, 4 (2011), 38:1–38:18.
- [45] Chicago Taxi Trips. 2019. City of Chicago Data Portal. <https://data.cityofchicago.org/Transportation/Taxi-Trips-2019/h4cq-z3dy>.
- [46] Ashish Vaswani, Noam Shazeer, Niki Parmar, Jakob Uszkoreit, Llion Jones, Aidan N. Gomez, Lukasz Kaiser, and Illia Polosukhin. 2017. Attention is All you Need. In *NeurIPS*. 5998–6008.
- [47] Petar Velickovic, Guillem Cucurull, Arantxa Casanova, Adriana Romero, Pietro Liò, and Yoshua Bengio. 2018. Graph Attention Networks. In *ICLR*. OpenReview.net.
- [48] Bao Wang, Duo Zhang, Duanhao Zhang, P. Jeffery Brantingham, and Andrea L. Bertozzi. 2019. Deep Learning for Real-Time Crime Forecasting and Its Ternarization. *Chinese Annals of Mathematics, Series B* 40 (2019), 949–966.
- [49] Hongjian Wang, Porter Jenkins, Hua Wei, Fei Wu, and Zhenhui Li. 2019. Learning Task-Specific City Region Partition. In *WWW*. ACM, 3300–3306.
- [50] Hongjian Wang, Daniel Kifer, Corina Graif, and Zhenhui Li. 2016. Crime Rate Inference with Big Data. In *SIGKDD*. ACM, 635–644.
- [51] Hongjian Wang, Huaxiu Yao, Daniel Kifer, Corina Graif, and Zhenhui Li. 2019. Non-Stationary Model for Crime Rate Inference Using Modern Urban Data. *IEEE Trans. Big Data* 5, 2 (2019), 180–194.
- [52] Sarah Wiegrefe and Yuval Pinter. 2019. Attention is not not Explanation. In *EMNLP-IJCNLP*. Association for Computational Linguistics, 11–20.
- [53] Chuanxiu Xiong, Ajitesh Srivastava, Rajgopal Kannan, Omkar Damle, Viktor K. Prasanna, and Erroll Southers. 2019. On Predicting Crime with Heterogeneous Spatial Patterns: Methods and Evaluation. In *SIGSPATIAL*. ACM, 43–51.
- [54] Kelvin Xu, Jimmy Ba, Ryan Kiros, Kyunghyun Cho, Aaron C. Courville, Ruslan Salakhutdinov, Richard S. Zemel, and Yoshua Bengio. 2015. Show, Attend and Tell: Neural Image Caption Generation with Visual Attention. In *ICML*. JMLR.org, 2048–2057.
- [55] Huaxiu Yao, Xianfeng Tang, Hua Wei, Guanjie Zheng, and Zhenhui Li. 2019. Revisiting Spatial-Temporal Similarity: A Deep Learning Framework for Traffic Prediction. In *AAAI*. AAAI Press, 5668–5675.
- [56] Huaxiu Yao, Fei Wu, Jintao Ke, Xianfeng Tang, Yitian Jia, Siyu Lu, Pinghua Gong, Jieping Ye, and Zhenhui Li. 2018. Deep Multi-View Spatial-Temporal Network for Taxi Demand Prediction. In *AAAI*. AAAI Press, 2588–2595.
- [57] Chung-Hsien Yu, Wei Ding, Ping Chen, and Melissa Morabito. 2014. Crime Forecasting Using Spatio-temporal Pattern with Ensemble Learning. In *PAKDD*. Springer, 174–185.
- [58] Junbo Zhang, Yu Zheng, and Dekang Qi. 2017. Deep Spatio-Temporal Residual Networks for Citywide Crowd Flows Prediction. In *AAAI*. AAAI Press, 1655–1661.
- [59] Junbo Zhang, Yu Zheng, Dekang Qi, Ruiyuan Li, and Xiuwen Yi. 2016. DNN-based prediction model for spatio-temporal data. In *SIGSPATIAL*. ACM, 92:1–92:4.
- [60] Xiangyu Zhao and Jiliang Tang. 2017. Modeling Temporal-Spatial Correlations for Crime Prediction. In *CIKM*. ACM, 497–506.